Indonesian Journal of Electrical Engineering and Informatics (IJEEI)
Vol. 13, No. 2, June 2025, pp. 368∼386
ISSN: 2089-3272, DOI: 10.52549/ijeei.v13i2.6209

Closed-Form Solution for Energy Efficiency Maximization in Uplink IRS-Assisted Multi-User NOMA Network

El-Hadi Meftah[1], Slimane Benmahmoud[2]
[1]LISIC Laboratory, Faculty of Electrical Engineering, USTHB, Algiers, Algeria
[2]Department of Electronics Engineering, Mohamed Boudiaf University, M'sila, Algeria

Article Info

Article history:

Received Jan 3, 2025
Revised Apr 26, 2025
Accepted May 13, 2025

Keywords:

Energy efficiency (EE)
intelligent reflecting surface (IRS)
non-orthogonal multiple access (NOMA)
power consumption
spectral efficiency (SE)

ABSTRACT

Given the growing concerns about energy consumption and its negative impact on the ecosystem, energy efficiency (EE) has become one of the most important key performance indicators in current and future wireless communication technologies. In this paper, we address the EE maximization problem in an uplink intelligent reflective surface (IRS)-assisted multi-user non-orthogonal multiple access (NOMA) network. This problem is formulated as a trade-off between the spectral efficiency (SE) and total power consumption, and it appears to be non-convex. To avoid the complexity associated with the traditional iteration-based Dinkelbach method, we opt for an alternative closed-form solution for the users' transmit power based on partial derivative analysis and Lambert function. Simulation results with a realistic power consumption models confirm the accuracy of our theoretical findings.

Corresponding Author:

El-Hadi Meftah
LISIC Laboratory, Faculty of Electrical Engineering, University of Science and Technology Houari Boumediene,
BP 32 Bab Ezzouar, Algiers, Algeria
Email: emeftah@usthb.dz

1. INTRODUCTION

The evolution of information and communication technologies (ICTs), especially the mass deployment of 5G, is driving significant changes in the wireless communications landscape. Indeed, the rapid increase in the number, and diversity of connected devices [1][1], data traffic and supported applications is raising concerns about its impact on the environment, notably in terms of greenhouse gas (GHG) emissions. The trend shows that the ICTs sector contributes between 1.5% and 4% of worldwide GHG emissions[2, 3]. Furthermore, forecasts indicate that by 2040, GHG emissions generated by ICTs could account for over 16% of worldwide emissions, with a significant proportion coming from end-user devices [3]. In light of these facts, it is essential to investigate innovative approaches to develop green technological solutions aimed at mitigating environmental impacts and promoting sustainability. This involves integrating more eco-friendly energy sources and improving energy efficiency (EE).

One such innovative approaches aimed at improving EE leverages the integration of intelligent reflective surfaces (IRSs) [4]. IRS is a flat structure composed of a large number of passive, cost-effective and energy-efficient reflecting elements, which deviate from traditional reflection laws to adjust the phase and direction of electromagnetic waves, enabling precise and controlled reflection or refraction. In addition, the IRS has the ability to adapt dynamically and instantaneously to the variations in the wireless channel by modifying

[1]The 5G subscriptions keep growing fast, from 1.6 billion in 2023 to 2.27 billion in 2024, with a forecast of 6.35 billion by 2030.

the phase shifts and/or amplitudes of its elements. As a result, the incident signals can be redirected according to the system's overall performance targets. Owing to their passive nature, IRSs require less energy consumption compared with conventional relays [5]. Thanks to this EE, IRSs are a crucial innovation for future green wireless communication systems [6].

Another promising technology for next-generation wireless networks is non-orthogonal multiple access (NOMA), meeting the requirements for massive connectivity, high spectral efficiency (SE), and improved EE [7–9]. Unlike traditional orthogonal multiple access (OMA) schemes, NOMA allows multiple users equipments (UEs) to share the same degrees of freedom, so that UEs are served on the same radio resources by superimposing their signals at the transmitter-end and decoding these signals at the receiver-end using successive interference cancellation (SIC) [10, 11]. In addition, the use of NOMA leads to a significant improvement in the system EE and SE compared to OMA. Nevertheless, this improvement is only achieved when the users' channel strengths exhibit significant differences, which is not necessarily the case in real communication situations. In light of the above, IRS can be effectively combined with NOMA to improve the overall system's performance, where IRS can artificially provide extra paths to boost a specific user's channel gain, thereby improving the SIC performance[12]. This synergy is often referred to as IRS-aided NOMA[13], IRS-assisted NOMA[14] or merely IRS-NOMA [15].

Several studies have been conducted on optimizing the EE in IRS-assisted NOMA downlink communication [14, 16–20]. However, those dealing with uplink scenario are relatively limited. G. Li et *al*. [21] proposed an iterative approach to solve the multivariate non-convex optimization problem to maximize system EE in IRS-empowered multiple input multiple-output (MIMO)-NOMA uplink systems. The approach involves the joint optimization of passive beamforming (BF) at the IRS, active BF at the base station (BS), and power allocation (PA). A comparison with baseline schemes shows a substantial gain in terms of system EE. In [22], the authors examined the joint optimization of users' transmit power, passive BF at the IRS and active BF at the BS, with a view to maximizing overall system EE in IRS-assisted multi-antenna NOMA uplink systems, while meeting users' minimum throughput constraints. To solve the highly challenging non-convex optimization problem, they developed an iterative solution using a block coordinate descent (BCD) approach. In [23], the authors sought to maximize EE for IRS-assisted millimeter-wave (mmWave) NOMA networks while considering constraints such as each device's minimum rate, maximum power and constant modulus (CM) of BF vectors. For this purpose, they presented two iterative algorithms: the first, based on majorization-minimization (MM), the concave-convex procedure (CCCP) and the BCD method, to obtain closed-form solution for the joint BF design problem; the second, based on successive convex approximation (SCA), BCD and Dinkelbach's methods, to achieve suboptimal closed-form PA for each iteration, given the designed passive and analog BFs. Recently, T. Qiao et *al* [24]. investigated EE maximization in a NOMA uplink system assisted by an active IRS, where reflecting elements amplified incident signals. Unlike conventional passive IRS architectures, their approach employed a cascaded channel-based user scheduling algorithm and jointly optimized transmit PA and active IRS's BF using Dinkelbach's method combined with SDR. Their results demonstrated substantial EE gains over passive IRS benchmarks, albeit at the expense of increased computational complexity and additional power consumption from active amplification.

Apart from the aforementioned studies, the EE maximization in the context of uplink IRS-assisted NOMA for mobile edge computing (MEC) and coordinated multipoint (CoMP) systems was investigated in [25] and [26], respectively. The authors in [25] aimed to minimize total energy consumption by jointly optimizing transmission time, offloading sharing and IRS phase shifts as well as transmit powers. They derived an optimal solution for transmit power in closed form and used an alternative optimization (AO) technique to solve the formulated problem. The authors in [26] investigated a transmit power minimization problem, which was further solved by leveraging an alternating method to iteratively optimize both transmit power and phase shifts.

In the previous studies, maximizing EE proved challenging due to the fractional form of its objective function. To overcome this, numerical fractional programming methods, such as the conventional Dinkelbach' method, were adopted[27]. This method aims to simplify the EE maximization problem by transforming it into a series of iterative non-linear problems. However, it frequently requires multiple unpredictable iterations, thereby increasing the overall computational complexity, especially for high-dimensional problems[28]. Furthermore, in the absence of a closed-form solution, the proposed methods are inadequate since they do not provide a sufficiently detailed analytical insight into the problem. To the best of our knowledge, none of these studies has provided a closed-form expression for the EE maximization and the EE-SE tradeoff. Such an expression is crucial for real-time communications as it helps in avoiding the high latency caused by the aforementioned methods. Therefore, in this paper, we derive closed-form expressions for the optimal users' transmit power maximizing the system EE in an uplink IRS-assisted multi-user NOMA network. To this end, we first derive the partial derivative of the objective function, and then formulate a closed-form solution for the transmit power using the Lambert function[29]. The main contributions in this work are listed as follows:

- Alongside the derivation of the closed-form expressions for the optimal users' transmit power maximizing the system EE, we also provide the corresponding expressions for their EE and SE in a way that the EE-SE trade-off is easily examined. Before doing so, we analyze the system EE based on both constant circuit power (CCP) and variable circuit power (VCP) models.
- To gain deeper insights, we further derive the asymptotic behavior of the optimal transmit power, system EE and SE when key system parameters (such as system bandwidth, maximum transmit power, number of IRS reflective elements, and static power dissipation (PD) of the hardware components) grow large.
- We extend our system model to a more realistic scenario involving a MIMO setup, demonstrating that in this context, the benefits of having a larger number of BS antennas in terms of system EE and SE can be faded by an increase in the amount of static PD of the hardware components.
- We provide extensive simulation results to verify the accuracy and correctness of the derived analysis for both circuit power models. In addition, we consider realistic simulation parameters, as listed in Table 1, and model the channel gains according to the 3GPP Urban Micro (UMi) model in [30, Table B.1.2.1-1]. Interestingly, we notice a perfect match between simulation and analytical results for all simulation sets.

The rest of this paper is structured as follows. In Section 2., we present the system model and problem formulation. The proposed solution for maximizing the EE is provided in Section 3., where we introduce realistic power consumption models for an IRS-assisted multi-user NOMA uplink network. These models are then used to derive closed-form expressions. In Section 4., we provide the simulation results to verify the accuracy of the analytical results. Finally, we draw some conclusions in Section 5..

Notations: we denote scalars by lower-case letters, while vectors and matrices are denoted by boldface lower-case and upper-case letters, respectively. We denote by $\boldsymbol{a}^{\mathrm{H}}$ and $\mathrm{diag}\left[\boldsymbol{a}\right]$ the Hermitian and the diagonal matrix of vector $\boldsymbol{a}$, respectively. $\arg\left(\bullet\right)$, $|\bullet|$ denotes the argument and the modulus of a complex number, respectively.

2. SYSTEM MODEL AND PROBLEM FORMULATION

2.1. System Model

In this work, we consider an uplink IRS-assisted multi-user NOMA network in which K single-antenna UEs aim to communicate with a single-antenna BS, as illustrated in Fig. 1. Due to poor propagation conditions, we have neglected the direct link between the BS and the UEs. Therefore, to ensure such communication, we resort to an IRS with N reflective elements. Thus, the signal received at the BS can be expressed as

$$\begin{aligned} y &= \sum_{k=1}^{K} \mathbf{h}_{\mathrm{BS}}^{H} \mathbf{\Phi} \mathbf{h}_k \sqrt{p_k} x_k + w \qquad (1) \\ &= \mathbf{h}_{\mathrm{BS}}^{H} \mathbf{\Phi} \mathbf{h}_k \sqrt{p_k} x_k + \sum_{i=1, i\neq k}^{K} \mathbf{h}_{\mathrm{BS}}^{H} \mathbf{\Phi} \mathbf{h}_i \sqrt{p_i} x_i + w, \end{aligned}$$

where x_k stands for the unit-power transmitted signal of UE$_k$, i.e., $\mathbb{E}\left\{|x_k|^2\right\} = 1$, $\forall k \in \mathcal{K}$, where $\mathbb{E}\left\{\cdot\right\}$ denotes the expectation operator, and the set $\mathcal{K}$ is given by $\mathcal{K} \triangleq \{1, \cdots, K\}$. p_k denotes the transmit power of UE$_k$. $\mathbf{h}_k \in \mathbb{C}^{N\times 1}$ and $\mathbf{h}_{\mathrm{BS}} \in \mathbb{C}^{N\times 1}$ are respectively the fading vectors of the UE$_k$ $\rightarrow$IRS and IRS$\rightarrow$BS links. $\mathbf{\Phi} = \mathrm{diag}[\kappa_1\phi_1, \kappa_2\phi_2, \cdots, \kappa_N\phi_N]$ is the phase-shift matrix comprising the response of all IRS reflecting elements, where $\kappa_n \in [0, 1]$ is the amplitude reflection coefficient, while $\phi_n = \mathrm{e}^{j\theta_n}, j = \sqrt{-1}$, $\theta_n \in [0, 2\pi)$, $\forall n \in \mathcal{N}$, and the set $\mathcal{N}$ is given by $\mathcal{N} \triangleq \{1, \cdots, N\}$, represents the phase shift caused by the n^{th}-element of

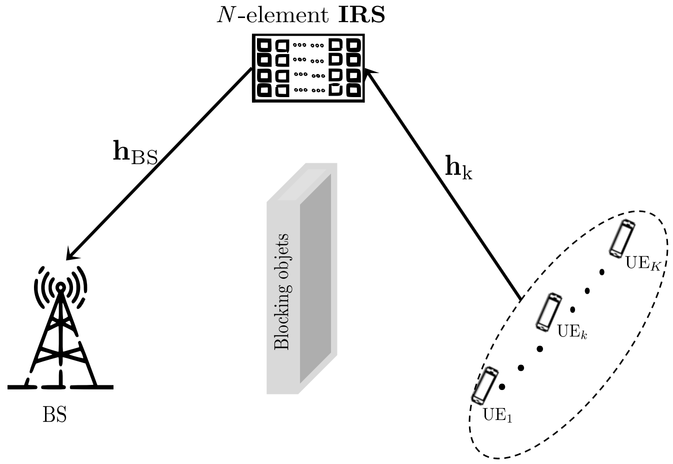

Figure 1. Uplink IRS-assisted multi-user NOMA network.

the IRS unit. $w \sim \mathcal{CN}(0, \sigma^2)$ denotes the zero-mean additive white Gaussian noise (AWGN) at the BS, with a variance σ^2.

As in a conventional uplink NOMA network, the BS applies SIC decoding strategy to decode the UEs' signals. To begin with, UEs must be sorted according to their effective channel gains, so that those with the best channel conditions are decoded first. Here, the effective channel for user k is

$$\mathbf{h}_{\mathrm{BS}}^H \mathbf{\Phi} \mathbf{h}_k = \sum_{n=1}^{N} \kappa_n \mathrm{e}^{j\theta_n} h_{\mathrm{BS},n} h_{k,n}$$

. where $h_{\mathrm{BS},n}$ and $h_{k,n}$ are the n^{th}-elements of $\mathbf{h}_{\mathrm{BS}}$ and $\mathbf{h}_k$, respectively. The links are assumed to undergo Nakagami $-m$ fading, i.e., $|\mathbf{h}_{\mathrm{BS},n}| \sim \mathrm{Nakagami}\,(m_{\mathrm{BS}}, \Omega_{\mathrm{BS}})$, and $|\mathbf{h}_{k,n}| \sim \mathrm{Nakagami}\,(m_{\mathbf{h}_k}, \Omega_{\mathbf{h}_k})$, where $(m_{\mathrm{BS}}, \Omega_{\mathrm{BS}})$, and $(m_{\mathbf{h}_k}, \Omega_{\mathbf{h}_k})$ are the corresponding distribution parameters. Furthermore, we assume that the channel state information (CSI) of all links is perfectly known to the BS and IRS controller and can be estimated using existing methods such as [31–33]. For the sake of simplicity, we assume that the UEs are ordered in a descending order of their effective channel gains, i.e.,

$$|\mathbf{h}_{\mathrm{BS}}^H \mathbf{\Phi} \mathbf{h}_1|^2 \geq \cdots \geq |\mathbf{h}_{\mathrm{BS}}^H \mathbf{\Phi} \mathbf{h}_K|^2. \tag{2}$$

Following the SIC decoding procedure, the signal-to-interference plus noise ratio (SINR) of UE$_k$ can be expressed as [34]

$$\mathrm{SINR}_k \triangleq \frac{|\mathbf{h}_{\mathrm{BS}}^H \mathbf{\Phi} \mathbf{h}_k|^2 p_k}{\sum_{i=k+1}^{K} |\mathbf{h}_{\mathrm{BS}}^H \mathbf{\Phi} \mathbf{h}_i|^2 p_i + \sigma^2}, \tag{3}$$

where $\sum_{i=k+1}^{K} |\mathbf{h}_{\mathrm{BS}}^H \mathbf{\Phi} \mathbf{h}_i|^2 p_i = 0$ for $k = K$.

Remark 1. *It should be noted that when designing the IRS, we adopt the idea of providing maximum gain to the prioritized UE, i.e., the first user in our case, so as to maximize its received SNR. Consequently, the optimal continuous phase shifts can be obtained as follows* $\mathbf{\Phi} = -\arg\left(\mathbf{h}_{\mathrm{BS},n} \mathbf{h}_{1,n}\right)$*, and UE*$_1$*'s equivalent channel after adopting this phase-shift configuration is given by* $\left|\mathbf{h}_{\mathrm{BS}}^H \mathbf{\Phi} \mathbf{h}_1\right| = \kappa \left|\sum_{n=1}^{N} \mathrm{e}^{j\theta n} \mathbf{h}_{\mathrm{BS},n}\, \mathbf{h}_{1,n}\right| = \kappa \sum_{n=1}^{N} |\mathbf{h}_{\mathrm{BS},n}|\, |\mathbf{h}_{1,n}|$*. Here, we assume that* $\kappa_n = \kappa$*,* $\forall n \in \mathcal{N}$*.*

2.2. Problem Formulation

To facilitate the presentation of the problem formulation, we introduce the following basic definitions.

Definition 1. *Based on* (3)*, the system SE in bps/Hz is given by*

$$\begin{aligned}\mathcal{R} &\triangleq \sum_{k=1}^{K} \log_2\left(1+\frac{|\mathbf{h}_{\mathrm{BS}}^{H}\mathbf{\Phi}\mathbf{h}_k|^2 p_k}{\sum_{i=k+1}^{K}|\mathbf{h}_{\mathrm{BS}}^{H}\mathbf{\Phi}\mathbf{h}_i|^2 p_i+\sigma^2}\right) \\ &\overset{(a)}{=} \log_2\left(1+\frac{\sum_{k=1}^{K}|\mathbf{h}_{\mathrm{BS}}^{H}\mathbf{\Phi}\mathbf{h}_k|^2 p_k}{\sigma^2}\right),\end{aligned} \tag{4}$$

where (a) *holds since the terms within the* $\log_2(\cdot)$ *function create a telescoping product.*

To simplify our analytical framework, we assume an equal resource allocation strategy for the NOMA scheme. Indeed, previous research, including [35],[36], and [4], has shown that it is not always necessary to allocate extra power to users with poorer channel conditions. This assumption is particularly suitable for applications with minimal system overhead requirements, such as the Internet of Things (IoT) and machine-to-machine (MTC) communication networks.
Therefore, let's assume $p_k = \frac{P_{max}}{K}, \forall k$, and $\sum_{k=1}^{K} p_k = P_{max}$, P_{max} is the total power limit, the (4) becomes

$$\begin{aligned}\mathcal{R} &= \log_2\left(1+\frac{P_{max}}{K\sigma^2}\sum_{k=1}^{K}|\mathbf{h}_{\mathrm{BS}}^{H}\mathbf{\Phi}\mathbf{h}_k|^2\right) \\ &= \log_2\left(1+\frac{P_{max}}{K\sigma^2}\beta\right),\end{aligned} \tag{5}$$

where $\beta = \sum_{k=1}^{K}|\mathbf{h}_{\mathrm{BS}}^{H}\mathbf{\Phi}\mathbf{h}_k|^2$ represents the sum of all UEs effective channel gains.

Remark 2. *According to* (5)*, the system SE is a function of* β*, which in turn is independent of UEs' ordering. Therefore, we can state that the system SE for uplink IRS-assisted multi-user NOMA network is also independent of SIC ordering.*

Definition 2. *The system EE is defined as [5]*

$$\Theta = B\frac{\mathcal{R}}{\mathcal{P}_{total}}[\,\textit{bit/Joule}], \tag{6}$$

where B *is the overall system bandwidth, and* $\mathcal{P}_{total}$ *is the total power consumed by the system.*

Given the considered system model, we aim to find the optimal transmit power scheme that maximizes the system EE in (6). Mathematically, this can be formulated as follows

$$\mathbb{P}0: \quad \max_{P_{max}} \Theta \tag{7}$$

$$\text{s.t.} \quad P_{max} \le P_{peak}, \tag{C1}$$

$$\mathbf{\Phi} = -\arg\left(\mathbf{h}_{\mathrm{BS},n}\mathbf{h}_{1,n}\right), \forall n \in \mathcal{N}, \forall k \in \mathcal{K}. \tag{C2}$$

Here, the constraint (C1) ensures that $\sum_{k=1}^{K} p_k$ does not exceed the maximum achievable threshold power P_{peak}. The constraint (C2) relates to the IRS phase shift matrix design. It is clear that problem $(\mathbb{P}0)$ is non-convex due to the fractional structure of the objective function and the non-convex constraints. The most commonn adopted method to solve $(\mathbb{P}0)$ is the fractional programming method using Dinkelbach's algorithm[27]. However, the latter suffers from high computational complexity. In fact, by applying Dinkelbach's approach, the fractional problem in (7) remains intractable. Therefore, the problem is transformed into a nonlinear programming problem for $\alpha \ge 0$, given by

$$\max_{P_{\max}} \left\{B\mathcal{R} - \alpha\mathcal{P}_{\text{total}}\right\}, \tag{8}$$

where α represents the Dinkelbach's parameter that tradeoff between $B\mathcal{R}$ and $\mathcal{P}_{\text{total}}$. The main challenge lies in the fact that this parameter is unknown, requiring repeated trials and an unpredictable number of iterations to achieve convergence.

Faced with this challenge, in the next section we directly consider the partial derivative of $(\mathbb{P}0)$ to derive a computationally efficient closed-form solution involving the Lambert function. This significantly reduces the complexity compared to the fractional programming methods commonly used in the literature, such as those of [37], and [38].

3. PROPOSED EE MAXIMIZATION

According to Definition 2, system EE optimization is grounded on the cost-benefit concept, which involves balancing the benefits of system SE against the costs of $\mathcal{P}_{\text{total}}$[39–41]. Thus, accurate and realistic models of $\mathcal{P}_{\text{total}}$ are crucial to accurately assess this balance, taking into account both hardware components and digital signal processing involved in the network. By incorporating these models into the analysis, effective optimization strategies can be devised to maximize system EE, thus ensuring efficient use of energy resources.

3.1. Constant circuit power

Under the assumptions of CCP, $\mathcal{P}_{\text{total}}$ includes both the transmit power $P_{\max}$ and the static PD of the hardware components P_{sta}. For the uplink IRS-assisted multi-user NOMA setup, it is given by [4], [24, 28]

$$\begin{aligned} \mathcal{P}_{\text{total}} &= \varepsilon \sum_{k=1}^{K} p_k + P_{\text{BS}} + KP_{\text{UE}} + NP_{\text{e}} \\ &= \varepsilon P_{max} + \underbrace{P_{\text{BS}} + KP_{\text{UE}} + NP_{\text{e}}}_{=P_{\text{sta}}}, \end{aligned} \tag{9}$$

wherein $\varepsilon \triangleq \mu^{-1}$ with $\mu \in (0,1]$ is the power amplifier efficiency. P_{BS} , P_{UE}, and P_e are the PDs of the hardware components at the BS, at the UE, and per each elements of the IRS unit, respectively. It should be noted that P_{sta} is modeled as a constant and that is independent of the system's bandwidth, and transmit power.

In case of CCP, the system SE in (5) can be rewritten as

$$\mathcal{R}_c = \log_2\left(1 + \varepsilon P_{max}\gamma\right), \tag{10}$$

with $\gamma = \frac{\beta}{\varepsilon K \sigma^2} = \frac{\beta}{\varepsilon K B N_0}$, and N_0 the noise power spectral density.

Furthermore, substituting (9) and (10) in (6), the corresponding EE yields

$$\Theta_c = B\frac{\log_2\left(1 + \varepsilon P_{max}\gamma\right)}{\varepsilon P_{max} + P_{sta}}. \tag{11}$$

The above formula reveals the dependence of the system EE on the transmit power as well as the bandwidth.

Corollary 1. *As P_{max} and/or B get larger, then $\Theta_c \approx \frac{\beta}{\ln(2)\varepsilon K N_0}$, where $\ln(\cdot)$ is the natural algorithm function.*

Proof. In (11), we assert that Θ_c is a monotonic, non-decreasing function of the bandwidth B, so that it is maximized as B tends to infinity. This boundary can be derived as

$$\lim_{B\to\infty} B\frac{\log_2\left(1 + P_{max}\frac{\beta}{KBN_0}\right)}{\varepsilon P_{max} + P_{sta}} = \frac{\beta}{\ln(2)\,\varepsilon K N_0}\frac{1}{\left(1 + \frac{P_{sta}}{\varepsilon P_{max}}\right)}. \tag{12}$$

A similar finding can be drawn from (12), which shows a monotonic increase as a function of the transmit power $P_{\max}$, allowing it to be maximized by taking $P_{\max}$ to infinity. We then obtain

$$\lim_{P_{max}\to\infty} \frac{\beta}{\ln(2)\,\varepsilon K N_0}\frac{1}{\left(1 + \frac{P_{sta}}{\varepsilon P_{max}}\right)} = \frac{\beta}{\ln(2)\,\varepsilon K N_0}. \tag{13}$$

□

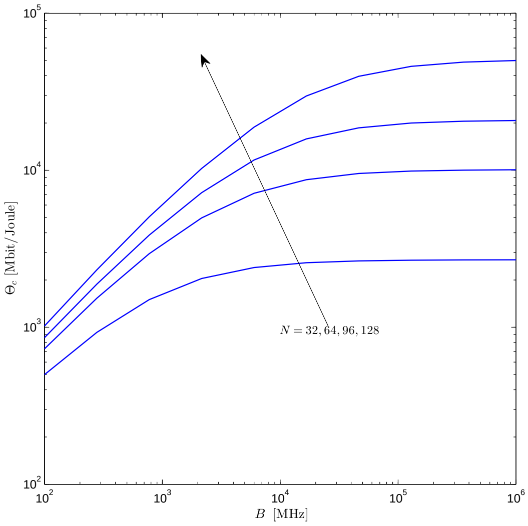

(a)

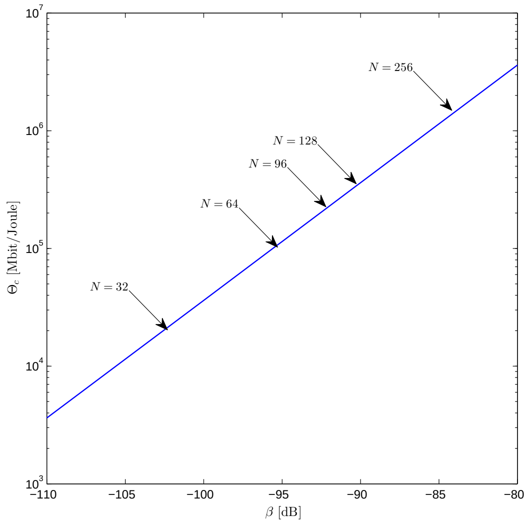

(b)

Figure 2. The system EE limit vs. (a) the bandwidth B, (b) the sum of UEs channel gains β.

Note that the result in (13) can be obtained when both $P_{\max}$ and B progress jointly to infinity, insofar as $P_{\max}$ has a slower convergence speed than B.

To evaluate the EE limit in (13), we plot it as a function of the bandwidth B in Fig. 2a, and the sum of all UE effective channel gains β in Fig. 2b. For clarity, we adopt the simulation parameters in Table 1. Fig. 2a illustrates the rate at which the UE reaches its limit when $B \to \infty$, for different values of N. For $N = 32$, this limit is reached at $B = 20\text{Ghz}$. However, it requires $5\times$ more bandwidth to reach the EE limit when doubling the size of the IRS unit, i.e., for $N = 64$. Furthermore, Fig. 2b shows that the EE limit increases monotonically with β, which is consistent with the finding in **Corollary** 1. The solid arrows in this figure indicate the values of N corresponding to fade levels. For example, when $N = 64$, we get $\beta = -95\text{dB}$.

Let us now focus on deriving the unique solution for determining the optimal transmit power $P^{\star}_{max}$ that maximizes Θ_c. To do so, Let us first consider the following **Lemma**.

Lemma 1. *Let a, b, c and $d \in \mathbb{R}^+$, and the function $f(x) = d\frac{\log_2(1+acx)}{ax+b}$. The global unique optimal solution that maximizes $f(x)$ is given by*

$$x^* = \frac{1}{ac}\left(\mathrm{e}^{\mathcal{W}\left(\frac{cb-1}{\mathrm{e}}\right)+1} - 1\right), \tag{14}$$

and its corresponding maxima is

$$f(x^*) = \frac{d}{\ln(2)}\frac{c}{\mathrm{e}^{\mathcal{W}\left(\frac{cb-1}{\mathrm{e}}\right)+1}}, \tag{15}$$

where $\mathcal{W}(\cdot)$ is the Lambert function defined as the inverse function of $x \mapsto xe^x$ [29], and e is the base of the natural logarithm function.

Proof. Please refer to Appendix A1.. □

Theorem 1. *The optimal transmit power that maximizes the system EE in* (11) *is given by*

$$P^{\star}_{max} = \frac{1}{\varepsilon\gamma}\left(\mathrm{e}^{\mathcal{W}\left(\frac{\gamma P_{sta}-1}{\mathrm{e}}\right)+1} - 1\right), \tag{16}$$

and the maximum system EE is

$$\Theta^{\star}_c = \frac{B}{\ln(2)}\frac{\gamma}{\mathrm{e}^{\mathcal{W}\left(\frac{\gamma P_{sta}-1}{\mathrm{e}}\right)+1}}. \tag{17}$$

Proof. This is a straightforward result of **Lemma** 1, for $a = \varepsilon$, $b = P_{sta}$, $c = \gamma$, and $d = B$. □

Remark 3. *Note that the Lambert function is increasing on* $\left[-\frac{1}{\mathrm{e}}, +\infty\right[$, *which holds true since,* $\frac{\gamma P_{sta}-1}{\mathrm{e}} \geq -\frac{1}{\mathrm{e}} \Rightarrow \gamma P_{sta} \geq 0$.

To deepen the analysis, we can relate the maximum system EE value (i.e., $\Theta_c^\star$) to its corresponding system SE (i.e., $\mathcal{R}_c^\star$). Plugging $P_{max}^\star$ in (10) yields

$$\mathcal{R}_c^\star = \frac{1}{\ln(2)}\left(\mathcal{W}\left(\frac{\gamma P_{sta}-1}{\mathrm{e}}\right)+1\right). \tag{18}$$

After some mathematical manipulations in (17) , we get the following equality

$$\log_2\left(\Theta_c^\star\right) + \mathcal{R}_c^\star = \log_2\left(\frac{\gamma B}{\ln(2)}\right). \tag{19}$$

In (19), $\log_2\left(\Theta_c^\star\right)$ and $\mathcal{R}_c^\star$ follow a linear dependence. We can therefore achieve an exponential gain in the system EE at the cost of a linear loss in the system SE.

Corollary 2. *As* γ *and/or* P_{sta} *get larger (i.e.,* $\gamma P_{sta} \gg 1$*), then*

$$\begin{aligned} P_{max}^\star &\approx \frac{1}{\varepsilon\gamma}\left(\frac{\gamma P_{sta}-1}{\mathrm{e}}\right) \\ &\approx \frac{P_{sta}}{\varepsilon \mathrm{e}}, \end{aligned} \tag{20}$$

and

$$\begin{aligned} \Theta_c^\star &\approx \frac{B}{\ln(2)}\frac{\gamma}{\frac{\gamma P_{sta}-1}{\mathrm{e}}} \\ &\approx \frac{B\mathrm{e}}{\ln(2)\,P_{sta}}, \end{aligned} \tag{21}$$

and

$$\mathcal{R}_c^\star \approx \log_2\left(\frac{\gamma P_{sta}}{\mathrm{e}}\right). \tag{22}$$

Proof. $\mathrm{e}^{\mathcal{W}(x)+1} \approx x$ for large values of x. □

Remark 4. *From* (20)*, and* (21)*, we can see that* $\Theta_c^\star$ *and* $P_{max}^\star$ *are linearly decreasing and increasing functions of* P_{sta}*, respectively. Both are also independent of the user channel conditions.*

3.2. Variable circuit power

In the previous subsection, P_{sta} is considered independent of system's bandwidth. This implies that circuit consumption remains constant with respect to the system's sampling rate, which in turn is directly related to B. In practice, however, the PD of the hardware components is strongly affected by the system's sampling frequency, as well as by the power consumed in backhaul transmission, digital signal processing, encoding/decoding, and so on. It is therefore much more practical to consider a model adapted to a VCP consumption scenario. Let us now present the adapted circuit power consumption model

$$\mathcal{P}_{\text{total}} = \varepsilon P_{\max} + \eta B \mathcal{R}_v + \underbrace{\vartheta B + K P_{\text{UE}} + N P_{\text{e}}}_{=P_{\text{sta}}}, \tag{23}$$

where $\eta, \vartheta \geq 0$ denote the hardware characteristic constants related to load-dependent power consumption and digital signal processing, respectively. Applying (6) in this scenario, we obtain the system EE as follows

$$\Theta_v = B\frac{\log_2\left(1+\varepsilon P_{max}\gamma\right)}{\varepsilon P_{\max} + \eta B \log_2\left(1+\varepsilon P_{max}\gamma\right) + P_{\text{sta}}}. \tag{24}$$

Similarly, to determine the optimal transmit power $P_{max}^\star$ that maximizes Θ_v, we rely on the following **Lemma**.

Lemma 2. *Let a, b, c, d, and $z \in \mathbb{R}^+$, and the function $f(x) = d\frac{\log_2(1+acx)}{ax+zd\log_2(1+acx)+b}$. The global unique optimal solution that maximizes the $f(x)$ is given by*

$$x^* = \frac{1}{ac}\left(\mathrm{e}^{\mathcal{W}\left(\frac{cb-1}{\mathrm{e}}\right)+1} - 1\right), \tag{25}$$

and, its corresponding maxima is

$$f(x^*) = d\frac{c}{\ln(2)\ \mathrm{e}^{\mathcal{W}\left(\frac{cb-1}{\mathrm{e}}\right)+1} + dzc}.$$

Proof. Please refer to Appendix A2.. □

Theorem 2. *The system EE in* (24) *is maximized for any values of $P^\star_{max}$ such that*

$$P^\star_{max} = \frac{1}{\varepsilon\gamma}\left(\mathrm{e}^{\mathcal{W}\left(\frac{\gamma P_{sta}-1}{\mathrm{e}}\right)+1} - 1\right), \tag{26}$$

and the corresponding maximum system EE is

$$\Theta^\star_v = B\frac{\gamma}{\ln(2)\ \mathrm{e}^{\mathcal{W}\left(\frac{\gamma P_{sta}-1}{\mathrm{e}}\right)+1} + B\eta\gamma}. \tag{27}$$

Inserting $P^\star_{max}$ into (10), yields

$$\mathcal{R}^\star_v = \frac{1}{\ln(2)}\left(\mathcal{W}\left(\frac{\gamma P_{sta}-1}{\mathrm{e}}\right) + 1\right). \tag{28}$$

Proof. The results of (26) and (27) can be readily derived from **Lemma** 2 , for $a = \varepsilon$, $b = P_{sta}$, $c = \gamma$, $z = \eta$ and $d = B$. □

Remark 5. *According to* (26), *we can see that $P^\star_{max}$ does not depend on the load-dependent power consumption (through η).*

Corollary 3. *As γ and/or P_{sta} get larger (i.e., $\gamma P_{sta} \gg 1$), then*

$$P^\star_{max} \approx \frac{P_{sta}}{\varepsilon \mathrm{e}}, \tag{29}$$

and

$$\Theta^\star_v \approx \frac{B\mathrm{e}}{\ln(2)\left(P_{sta} + B\eta\mathrm{e}\right)}, \tag{30}$$

and

$$\mathcal{R}^\star_v \approx \log_2\left(\frac{\gamma P_{sta}}{\mathrm{e}}\right). \tag{31}$$

Proof. Here one can follow the same steps as in **Corollary** 2. □

Remark 6. *We can draw the same conclusions as in Remarks 4, and 5 except that P_{sta} here is a function of B (through ϑ).*

Let us now develop the new EE−SE relationship. Substituting (28) in (27) yields

$$\Theta^\star_v = B\frac{\gamma}{\ln(2)\, 2^{\mathcal{R}^\star_v} + B\eta\gamma}. \tag{32}$$

Applying the logarithm to both sides, we obtain

$$\log_2\left(\Theta^\star_v\right) + \mathcal{R}^\star_v = \log_2\left(\frac{B\gamma}{\ln(2)}\right) - \log_2\left(1 + 2^{-\mathcal{R}^\star_v}\frac{B\eta\gamma}{\ln(2)}\right). \tag{33}$$

The EE−SE relationship in (33) takes the same form as (19), apart from the additional terms relating to the load-dependent power consumption components.

3.3. Massive MIMO systems

So far, we have focused on the single-input single-output (SISO) systems framework. We can extend the analysis to include massive MIMO systems. To keep it concise, we assume that the BS is equipped with M antennas serving K single-antenna UEs (where $M \gg K$). Then, the received signal vector at the BS in (1) becomes

$$\mathbf{y} = \sum_{k=1}^{K} \mathbf{H}_{\text{BS}}^{H} \mathbf{\Phi} \mathbf{h}_k \sqrt{p_k} x_k + \mathbf{w}, \tag{34}$$

where $\mathbf{w} \sim \mathcal{CN}(0, \sigma^2 \boldsymbol{I}_M)$ denotes the AWGN at the BS. $\mathbf{H}_{\text{BS}} \in \mathbb{C}^{N \times M}$ denotes the fading matrix of IRS$\rightarrow$BS link. For this configuration, the circuit's power consumption model becomes

$$\mathcal{P}_{\text{total}} = \varepsilon P_{\max} + \eta M B \mathcal{R}_v + \underbrace{\vartheta M B + K P_{\text{UE}} + N P_{\text{e}}}_{=P_{\text{sta}}}, \tag{35}$$

while its corresponding system EE is

$$\Theta_v = B \frac{\log_2 \left(1 + \varepsilon P_{max} \gamma\right)}{\varepsilon P_{\max} + \eta M B \log_2 \left(1 + \varepsilon P_{max} \gamma\right) + P_{\text{sta}}}, \tag{36}$$

with $\gamma = \frac{\beta}{\varepsilon K \sigma^2}$, and $\beta = \sum_{k=1}^{K} |\mathbf{H}_{\text{BS}}^{H} \mathbf{\Phi} \mathbf{h}_k|^2$.

Corollary 4. *The system EE in* (36) *is maximized for any values of $P_{max}^{\star}$ such that*

$$P_{max}^{\star} = \frac{1}{\varepsilon \gamma} \left(\mathrm{e}^{\mathcal{W}\left(\frac{\gamma P_{sta} - 1}{\mathrm{e}}\right) + 1} - 1 \right), \tag{37}$$

and the corresponding maximum system EE is

$$\Theta_v^{\star} = B \frac{\gamma}{\ln(2)\ \mathrm{e}^{\mathcal{W}\left(\frac{\gamma P_{sta} - 1}{\mathrm{e}}\right) + 1} + B M \eta \gamma}, \tag{38}$$

with

$$\mathcal{R}_v^{\star} = \frac{1}{\ln(2)} \left(\mathcal{W}\left(\frac{\gamma P_{sta} - 1}{\mathrm{e}} \right) + 1 \right). \tag{39}$$

Corollary 5. *As γ and/or P_{sta} get larger (i.e., $\gamma P_{sta} \gg 1$), then*

$$P_{max}^{\star} \approx \frac{P_{sta}}{\varepsilon \mathrm{e}} \tag{40}$$

and

$$\Theta_v^{\star} \approx \frac{B \mathrm{e}}{\ln(2) \left(P_{sta} + B M \eta \mathrm{e}\right)}, \tag{41}$$

and

$$\mathcal{R}_v^{\star} \approx \log_2 \left(\frac{\gamma P_{sta}}{\mathrm{e}} \right). \tag{42}$$

Proof. The **Corollaries** 4 and 5 can be easily deduced from **Lemma** 2 by setting $z = M\eta$. □

Here, the EE$-$SE relationship is given by

$$\Theta_v^{\star} = B \frac{\gamma}{\ln(2)\, 2^{\mathcal{R}_v^{\star}} + B M \eta \gamma}, \tag{43}$$

alternatively

$$\log_2 \left(\Theta_v^{\star}\right) + \mathcal{R}_v^{\star} = \log_2 \left(\frac{B\gamma}{\ln(2)} \right) - \log_2 \left(1 + 2^{-\mathcal{R}_v^{\star}} \frac{B M \eta \gamma}{\ln(2)} \right). \tag{44}$$

Table 1. Simulation parameters.

Parameters	Values	Parameters	Values
PD at BS [dBm]	39	Carrier frequency, f_c [Ghz]	2.5
PD at each UE [dBm]	10	Number of users, K	4
PD at IRS/elements [dBm]	10	Amplitude Reflection Coef., κ_n	$1, \forall k \in \mathcal{K}$
Efficiency factor $\forall k$	0.5	Nakagami shape parameter, m	$m_{\mathrm{BS}} = 4, m_{h_k} = 2.25, \forall k \in \mathcal{K}$
Noise power spectral density, N_0 [dBm/Hz]	-174	Antenna gains [dBi]	$G_{\mathrm{BS}} = G_{\mathrm{IRS}} = 5$, and $G_{\mathrm{UE}_k} = 0, \forall k \in \mathcal{K}$
Noise figure, NF [dBm]	10		
System bandwidh, B [Mhz]	10	$(x_{\mathrm{UE}_k}\,[\mathrm{m}], z_{\mathrm{UE}_k}\,[\mathrm{m}])$	$\sim \mathcal{U}\,[40, 80], \forall k \in \mathcal{K}$

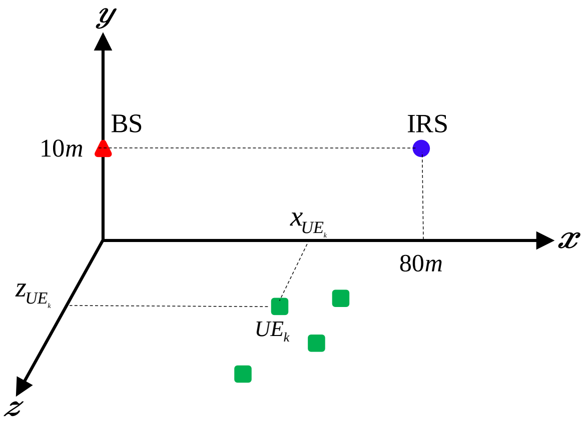

Figure 3. The relative positions of the BS, IRS and UEs in 3D coordinates.

4. SIMULATION RESULTS

In this section, we provide in-depth simulation results to validate the theoretical analysis presented in Section 3.. All simulations were performed using MATLAB $R2021b$ with the Symbolic Math Toolbox for Lambert-W computations,and execited on an Intel $i7-1185G7$ CPU @ 3.00202fGHz and 32202fGB RAM. For each scenario, we conducted Monte Carlo simulations with 10000 independent channel realizations to ensure statistical significance. In each run, we respectively position an IRS, and a BS in a three-dimensional (3D) Cartesian coordinate configuration (x, y, z) at : $(80\mathrm{m}, 10\mathrm{m}, 0\mathrm{m}), (0\mathrm{m}, 10\mathrm{m}, 0\mathrm{m})$, and whereas the UEs positions are randomly and uniformly distributed at $(x_{\mathrm{UE}_k}\,[\mathrm{m}], 0\mathrm{m}, z_{\mathrm{UE}_k}\,[\mathrm{m}])$, as shown in Fig. 3 [4]. Unless otherwise specified, we adopt the simulation parameters shown in Table 1, in which the equivalent AWGN power is $\sigma^2 = N_0 + 10\log_{10}(B) + NF$ [dBm]. We assume that all UEs→IRS→BS links experience $\mathrm{Nakagami} -m$ fading, and we model the large-scale path loss based on the 3GPP UMi parameters in [30, Table B.1.2.1-1] at a carrier frequency of 2.5 GHz. Moreover, we incorporated the path loss into the scale parameter of the $\mathrm{Nakagami} -m$ distribution as

$$\Omega_{\mathrm{t-r}}\,[\mathrm{dB}] = G_{\mathrm{t}} + G_{\mathrm{r}} - 28 - \log_{10}(f_c) - 22\log_{10}(d_{\mathrm{t-r}}/d_0), \tag{45}$$

where G_{t}, G_{r} denote, respectively, the transmit and receive antenna gains in [dBi] , and $d_{\mathrm{t-r}}$ [m] refers to the Euclidean distance for a specific link, while d_0 [m] represents the reference distance, in this case d_0 is set to $1\mathrm{m}$.

Fig. 4 plots the system EE versus system SE for $P_{\text{sta}} = \{0, 2, 4, 6, 8, 10, 12\}$ W. As we can see from Fig. 4a, in the absence of P_{sta}, i.e., $P_{\text{sta}} = 0$, we always have an increase in system SE at the expense of a decrease in system EE. In this case, moreover, the maximum EE is reached for communication with low SE, i.e., $\Theta_c^\star = \lim_{SE\to 0, P_{\text{sta}}=0} \Theta_c = \frac{\beta}{\ln(2)\varepsilon K N_0}$, note that we can find the same result by setting $P_{\text{sta}} = 0$ in (17), given that $\mathcal{W}\left(\frac{-1}{e}\right) = -1$. In practice, however, $P_{\text{sta}} > 0$, making EE a unimodal function that peaks at $\mathcal{R}_c^\star$ and decreases as SE gets larger. Indeed, in the low SNR regime, given that $\ln(1+x) \approx x$ for $x \to 0$, SE evolves almost linearly with P_{max}, while EE is primarily constrained by P_{sta}. Consequently, increasing P_{max} effectively increases both SE and EE. However, in the high SNR regime, P_{max} dominates the total energy consumption $\mathcal{P}_{\text{total}}$, so that the P_{sta} component in the denominator of (11) has no further influence. Furthermore, we can confirm the linear dependence between $\log_2(\Theta_c^\star)$ and $\mathcal{R}_c^\star$ derived from (19) via the red trade-off line. The slope of this line decreases as P_{sta} increases, primarily due to the necessity of augmenting transmit power (and consequently $\mathcal{R}_c$) to counterweigh its influence on Θ_c. The same reasoning can be followed for the VCP case illustrated in Fig. 4b.

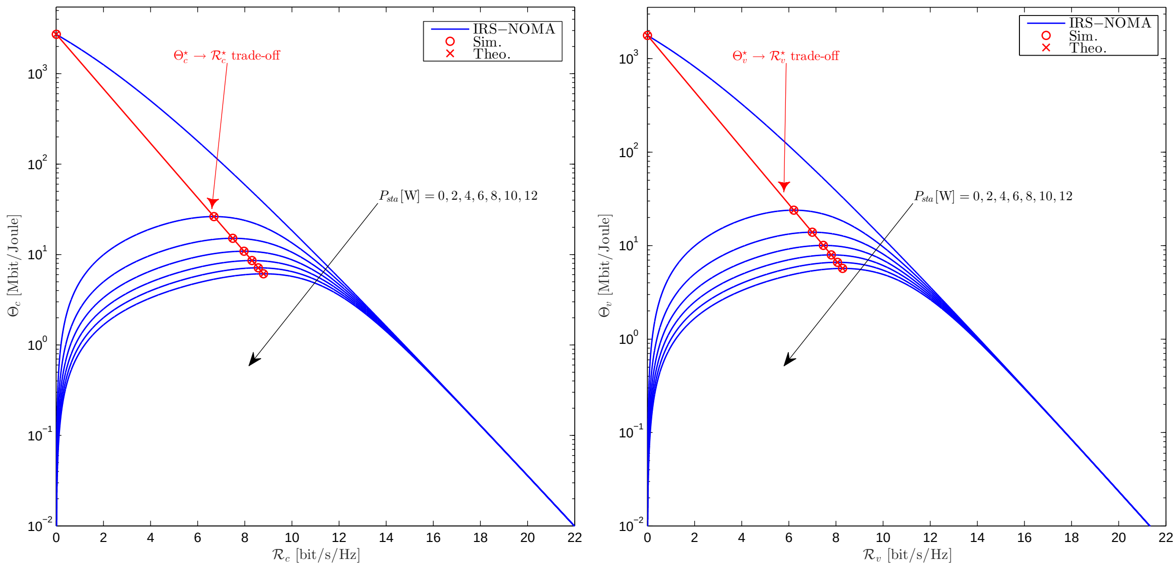

(a) (b)

Figure 4. The system EE vs. the system SE for different values of P_{sta} : (a) CCP, (b) VCP.

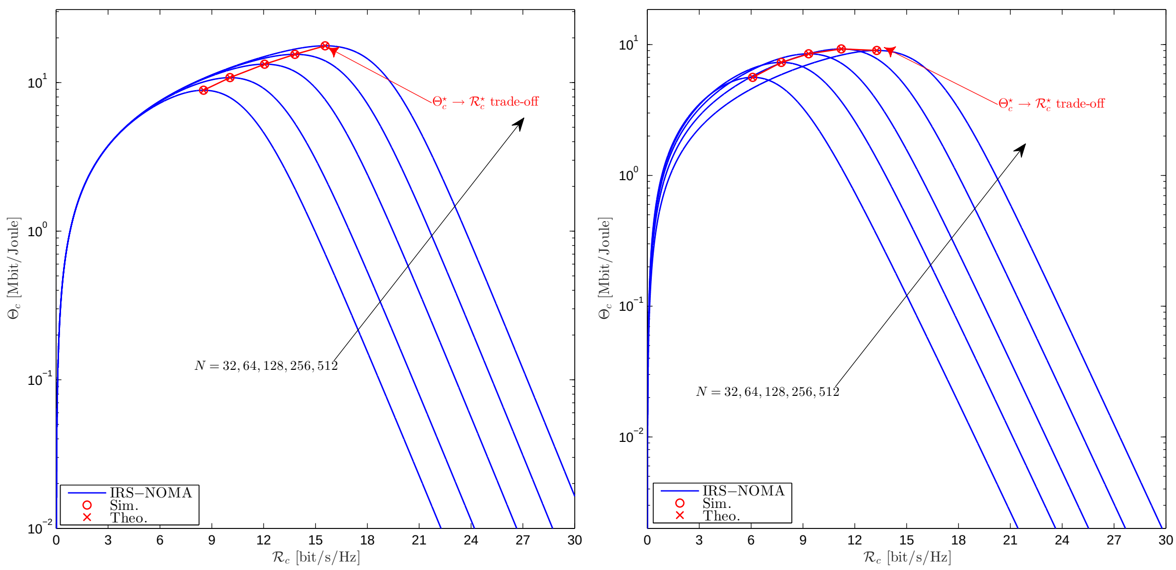

(a) (b)

Figure 5. The system EE vs. the system SE for different values of N, assuming CCP: (a) $P_{\text{e}} = 0$ W, (b) $P_{\text{e}} = 10$ dBm.

Fig. 5 shows the system EE as a function of the system SE for different values of N, assuming CCP. First, we assume that the PD at each IRS element is ignored, i.e. $P_{\text{e}} = 0$ W, making P_{sta} independent of N. As shown in Fig. 5a, the trade-off curve has a positive slope as N increases. Indeed, according to (18), since $\mathcal{W}(\cdot)$ is an increasing function for $x \geq \text{e}$, it follows that $\mathcal{R}_c^\star$ increases with N (given the fact that γ and β increase with N as already illustrated in Fig. 2b). Furthermore, $\Theta_c^\star$ in (17) increases unboundedly with N, as stated

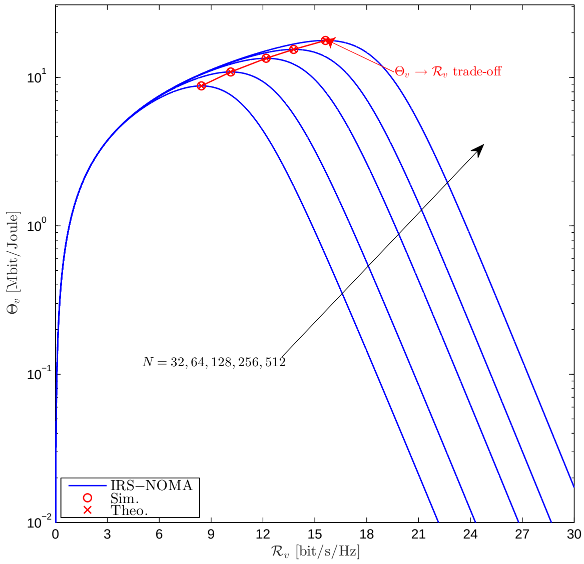

(a)

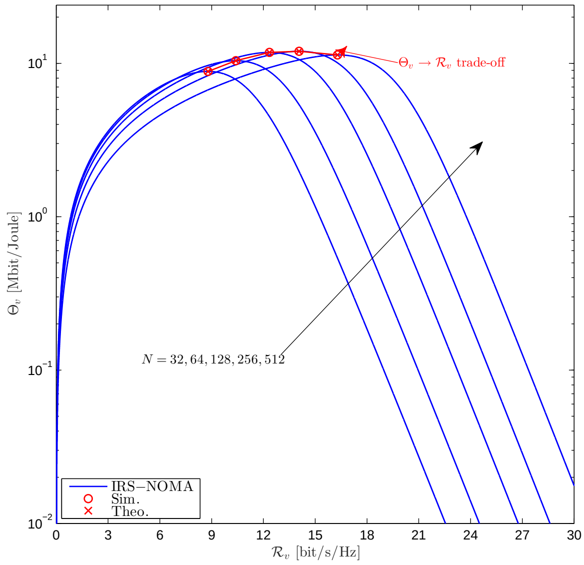

(b)

Figure 6. The system EE vs. the system SE for different values of N, assuming VCP: (a) $P_{\text{e}} = 0$ W, (b) $P_{\text{e}} = 10\ \text{dBm}$.

in **Corollary** 2. Now, assume that $P_{\text{e}} = 10\ \text{dBm}$. From Fig. 5b, the trade-off curve represents a unimodal function of N, showing a monotonic increase for $N \leq 256$ and a monotonic decrease for $N > 256$. As can be expected, $\mathcal{R}_c^\star$ always increases with N. However, the beneficial impact on $\mathcal{R}_c^\star$ quickly fades as each extra IRS element increases P_{sta}, leading to an unfavourable impact on $\Theta_c^\star$.

In Fig. 6, we conduct the same simulation as in Fig. 5 for the case of variable circuit power. Similarly, for $P_{\text{e}} = 0$ W, as shown in Fig. 6a, the trade-off curve has a positive slope as N increases. Furthermore, when $P_{\text{e}} = 10\ \text{dBm}$, depicted in Fig. 6b, the trade-off curve exhibits a unimodal function of N. Interestingly, in this case, P_{sta} is a modified form of ϑB compared to the one in the constant circuit power case in (9). We can therefore apply the same logic as in Fig. 5.

Fig. 7 shows the set of achievable system EE and system SE values in the case of variable circuit power, and for different values of P_{max} and B. The red line in Fig. 7a represents certain combinations of P and B yielding the maximum EE $\Theta_v^\star$ according to (26). Each of these combinations produces different system SE, as shown in Fig. 7b. Therefore, we can achieve any target system SE by varying P and B along the red line. For instance, for $\text{SNR} = P_{max}\gamma = -11$ dB, we can get a maximum EE of $124\ \text{Gbit/Joule}$ of and a system SE of 0.1 bits/s/Hz.

We proceed by further simulation for massive MIMO setup. To this end, we set $M = 64$. The results are shown in Fig. 8, with variable circuit power and the other parameters are same as those in Figs. 4b and 6. From this figure, it can be seen that with the increased M, there is a natural increase in the P_{sta} due to the additional hardware requirements and signal processing. Consequently, the benefits of a larger number of BS antennas in terms of system EE and SE can be faded by an increase in P_{sta}. In addition, as with the SISO setup, the trade-off curve exhibits a positive slope as N increase when $P_{\text{e}} = 0$ W, and it follows a unimodal function of N when $P_{\text{e}} = 10\ \text{dBm}$.

Table 2 summarizes the computational efficiency and performance gains of the proposed closed-form solution. The method outperforms existing approaches, including Dinkelbach iterative methods $\mathcal{O}\left(K^2\right)$ [24] and joint optimization method $\mathcal{O}\left(K^3\right)$ [19], achieving a significantly lower complexity of $\mathcal{O}\left(1\right)$ alongside superior EE (124 Gbit/Joule) with 70% lower latency (0.2 ms). Furthermore, these findings validate the proposed solution's ability to simultaneously minimize hardware requirements and maximize energy efficiency, making it particularly well-suited for real-time and resource-constrained scenarios such as IoT and URLLC.

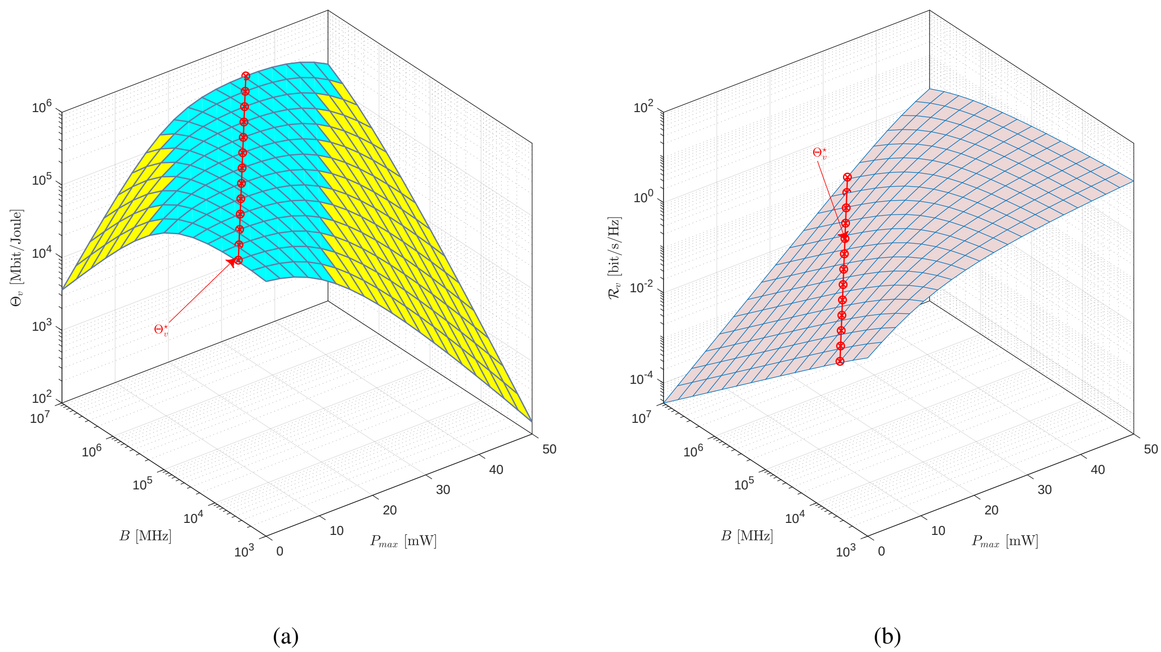

Figure 7. The system EE in (a), and the system SE in (b) as a function of P_{max} and B.

Table 2. Proposed vs. state-of-the-art performance comparison.

Metric	Proposed Method	[18]	[24]	[19]
Max EE (Gbit/Joule)	**124**	105	80	95
Computational Latency (ms)	**0.2**	1.5	2.1	1.8
Closed-Form Solution	**Yes**	No	No	No
Uplink Scenario	**Yes**	No	No	No

Remark 7. *The simulation results, illustrated by the circular markers in Fig. 4 to 8, align with the theoretical findings denoted by the cross markers obtained from Theorems 1 and 2.*

5. CONCLUSION

In this paper, we have investigated the EE maximization for uplink IRS-assisted multi-user NOMA network. Under perfect CSI assumption, we have derived a closed-form solution for the users' transmit power that allows an optimal trade-off between the achievable system EE and SE. We have also demonstrated the usefulness of our solution by alleviating the complexity associated with Dinkelbach's method, using the partial derivative and Lambert function. In addition, for performance comparison purposes, we have provided an asymptotic analysis for an upper bound on the theoretically achievable EE. Simulation results showed that the power consumption models have a significant impact on the system EE. Specifically, designing systems with reduced power consumption can significantly improve EE while maintaining the same system SE. Besides, the positive effect of increasing the number of IRS elements on the system SE is quickly neutralized by the P_{sta}'s negative effect on the system EE. Finally, future work will address minimum transmit power formulations with explicit rate constraints, leveraging the proposed closed-form solution. This extension is critical for practical scenarios requiring strict QoS and ultra-low energy consumption.

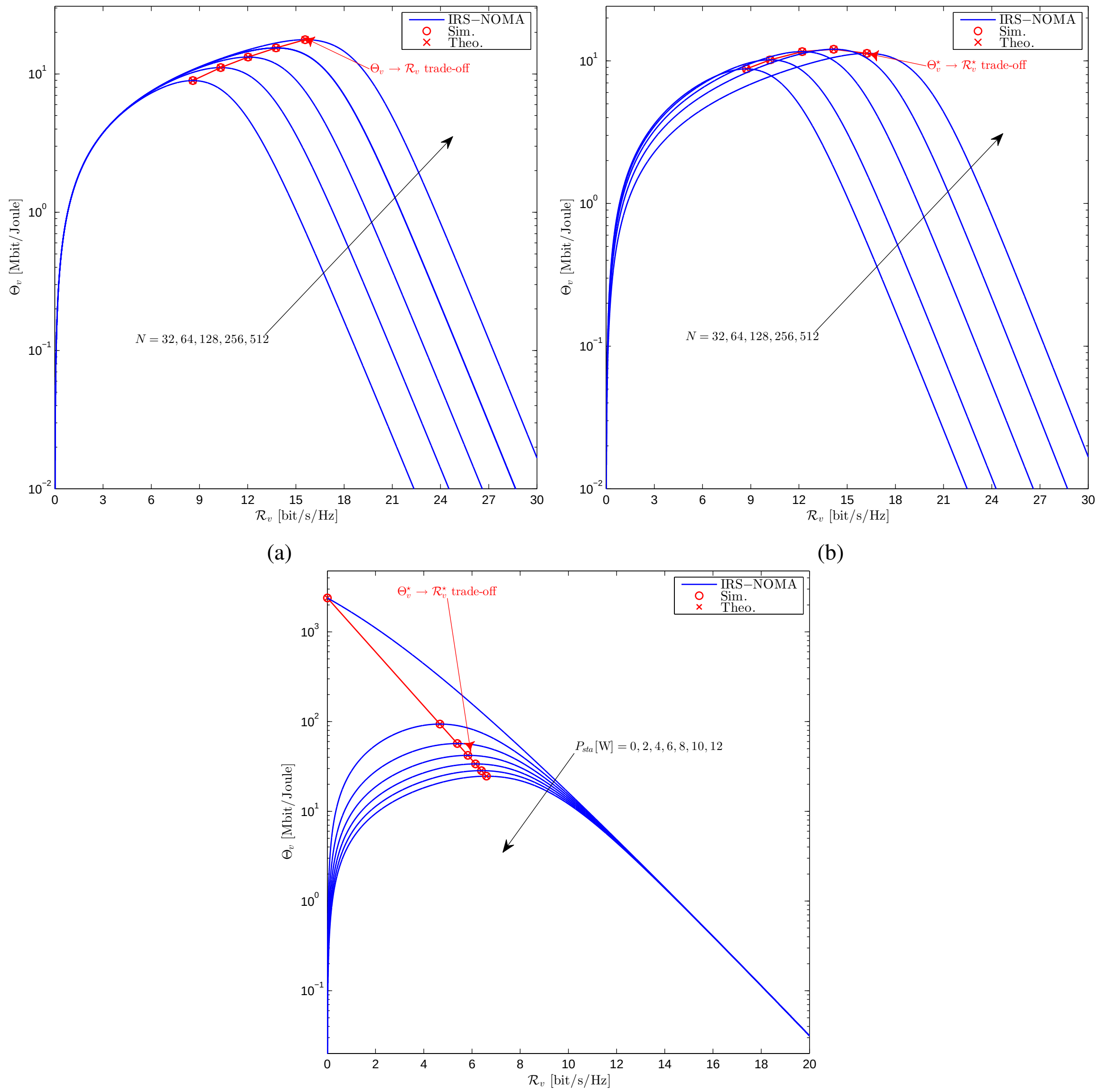

(a) (b) (c)

Figure 8. The system EE vs. the system SE for $M = 64$, assuming VCP: (a) varying N, $P_{\mathrm{e}} = 0$ W, (b) varying N, $P_{\mathrm{e}} = 10$ dBm, (c) varying P_{sta}.

A PROOFS OF LEMMAS

A1. Proof of Lemma 1

The numerator of the derivative of $f(x)$ is proportional to $g(x)$ which is given by

$$g(x) = -ad((acx + 1)\ln(acx + 1) - c(ax + b)). \tag{46}$$

The derivative of $g(x)$ is

$$\frac{dg(x)}{dx} = -a^2cd\ln(1 + acx) < 0. \tag{47}$$

This means that $g(x)$ is a monotonically decreasing function. The root x^* of $g(x)$ is found by solving $(1 + acx^*)\ln(1 + acx^*) = c(ax^* + b)$ and is given by

$$x^* = \frac{1}{ac}\left(e^{\mathcal{W}\left(\frac{cb-1}{e}\right)+1} - 1\right), \tag{48}$$

where $\mathcal{W}(.)$ is the Lambert W function. The maximum value of $f(x)$ is then

$$f(x^*) = \frac{d}{\ln(2)} \frac{c}{e^{\mathcal{W}\left(\frac{cb-1}{e}\right)+1}}. \tag{49}$$

A2. Proof of Lemma 2

Let us proceed with the same logic as for the proof **Lemma** 1, starting by finding the first derivative of the function $f(x)$ defined by

$$f(x) = d\frac{\log_2(1+acx)}{ax + zd\log_2(1+acx) + b}. \tag{50}$$

So, $\frac{\partial f(x)}{\partial x}$ is given in (51)

$$\frac{\partial f(x)}{\partial x} = u(x) - v(x) \tag{51}$$

where$u(x) = \frac{acd}{\ln(2)(acx+1)\left(\frac{zd\ln(acx+1)}{\ln(2)}+ax+b\right)}$, and$v(x) = \frac{d\ln(acx+1)\left(\frac{aczd}{\ln(2)(acx+1)}+a\right)}{\ln(2)\left(\frac{zd\ln(acx+1)}{\ln(2)}+ax+b\right)^2}$.

In this case, $g(x)$, the numerator of $\frac{\partial f(x)}{\partial x}$, can be expressed as

$$g(x) = ad\ln(2)(c(ax+b) - (acx+1)\ln(acx+1)), \qquad \forall x > 0 \tag{51}$$

and, $\frac{\partial g(x)}{\partial x}$ is

$$\frac{\partial g(x)}{\partial x} = -a^2cd\ln(2)\ln(1+acx) < 0, \tag{51}$$

when (A2.) holds, with $g(0) = abcd > 0$ and $\lim_{x\to\infty} g(x) = -\infty$. Hence, and similarly to the steps in (**??**), the global unique solution x^* necessarily corresponds to the maxima of $f(x)$ and is given by

$$x^* = \frac{1}{ac}\left(\mathrm{e}^{\mathcal{W}\left(\frac{cb-1}{\mathrm{e}}\right)+1} - 1\right). \tag{51}$$

After setting $\frac{\partial f(x)}{\partial x}$ in (51) to zero, and following some mathematical manipulations, we can obtain

$$\begin{aligned} f(x^*) &= \frac{cd}{dzc + \ln(2)(1+acx^*)} \\ &= \frac{cd}{dzc + \ln(2)\ \mathrm{e}^{\mathcal{W}\left(\frac{cb-1}{\mathrm{e}}\right)+1}}. \end{aligned} \tag{52}$$

ACKNOWLEDGMENTS

The authors would like to express their sincere gratitude to Dr. Ferdi Kara, of the Wireless Communication Technologies Laboratory (WCTLab), for his valuable contributions and insightful comments, which significantly contributed to the improvement of this work.

REFERENCES

[1] Ericsson, “Mobility report,” nov 2024. [Online]. Available: https://www.ericsson.com/en/reports-and-papers/mobility-report/reports/november-2024

[2] J. Bieser, R. Hintemann, S. Beucker, S. Schramm, L. Hilty, et al, and M. Kühn, “Klimaschutz durch digitale technologien ? chancen und risiken,” Berlin, Tech. Rep., 2020.

[3] J. C. Bieser, R. Hintemann, L. M. Hilty, and S. Beucker, “A review of assessments of the greenhouse gas footprint and abatement potential of information and communication technology,” *Environmental Impact Assessment Review*, vol. 99, p. 107033, 2023.

[4] C. Huang, A. Zappone, G. C. Alexandropoulos, M. Debbah, and C. Yuen, "Reconfigurable intelligent surfaces for energy efficiency in wireless communication," *IEEE Transactions on Wireless Communications*, vol. 18, no. 8, pp. 4157–4170, 2019.

[5] E. Björnson, Ö. Özdogan, and E. G. Larsson, "Intelligent reflecting surface versus decode-and-forward: How large surfaces are needed to beat relaying?" *IEEE Wireless Communications Letters*, vol. 9, no. 2, pp. 244–248, 2020.

[6] J. He, Y. Mao, Y. Zhou, T. Wang, and Y. Shi, "Reconfigurable intelligent surfaces empowered green wireless networks with user admission control," *IEEE Transactions on Communications*, vol. 71, no. 7, pp. 4062–4078, 2023.

[7] F. Fang, H. Zhang, J. Cheng, S. Roy, and V. C. M. Leung, "Joint user scheduling and power allocation optimization for energy-efficient NOMA systems with imperfect CSI," *IEEE Journal on Selected Areas in Communications*, vol. 35, no. 12, pp. 2874–2885, 2017.

[8] Y. Zhang, H.-M. Wang, T.-X. Zheng, and Q. Yang, "Energy-efficient transmission design in non-orthogonal multiple access," *IEEE Transactions on Vehicular Technology*, vol. 66, no. 3, pp. 2852–2857, 2017.

[9] H. Zhang, F. Fang, J. Cheng, K. Long, W. Wang, and V. C. M. Leung, "Energy-efficient resource allocation in NOMA heterogeneous networks," *IEEE Wireless Communications*, vol. 25, no. 2, pp. 48–53, 2018.

[10] S. M. R. Islam, N. Avazov, O. A. Dobre, and K.-s. Kwak, "Power-domain non-orthogonal multiple access (NOMA) in 5G systems: Potentials and challenges," *IEEE Communications Surveys Tutorials*, vol. 19, no. 2, pp. 721–742, 2017.

[11] Z. Ding, R. Schober, and H. V. Poor, "Unveiling the importance of SIC in NOMA systems—part 1: State of the art and recent findings," *IEEE Communications Letters*, vol. 24, no. 11, pp. 2373–2377, 2020.

[12] A. S. d. Sena, D. Carrillo, F. Fang, P. H. J. Nardelli, D. B. d. Costa, U. S. Dias, Z. Ding, C. B. Papadias, and W. Saad, "What role do intelligent reflecting surfaces play in multi-antenna non-orthogonal multiple access?" *IEEE Wireless Communications*, vol. 27, no. 5, pp. 24–31, 2020.

[13] W. Ni, X. Liu, Y. Liu, H. Tian, and Y. Chen, "Resource allocation for multi-cell IRS-aided NOMA networks," *IEEE Transactions on Wireless Communications*, vol. 20, no. 7, pp. 4253–4268, 2021.

[14] X. Yue and Y. Liu, "Performance analysis of intelligent reflecting surface assisted NOMA networks," *IEEE Transactions on Wireless Communications*, vol. 21, no. 4, pp. 2623–2636, 2022.

[15] Z. Ding and H. Vincent Poor, "A simple design of IRS-NOMA transmission," *IEEE Communications Letters*, vol. 24, no. 5, pp. 1119–1123, 2020.

[16] H. Wang, C. Liu, Z. Shi, Y. Fu, and R. Song, "On power minimization for IRS-aided downlink NOMA systems," *IEEE Wireless Communications Letters*, vol. 9, no. 11, pp. 1808–1811, 2020.

[17] F. Fang, Y. Xu, Q.-V. Pham, and Z. Ding, "Energy-efficient design of IRS-NOMA networks," *IEEE Transactions on Vehicular Technology*, vol. 69, no. 11, pp. 14 088–14 092, 2020.

[18] J. Wang and J. Li, "Energy efficiency maximization for irs-assisted noma networks," *Physical Communication*, vol. 52, p. 101647, 2022.

[19] K. H. Altuwairgi, A. M. T. Khel, and K. A. Hamdi, "On the performance of IRS-assisted multi-user THz-NOMA under beam misalignment," *IEEE Transactions on Vehicular Technology*, vol. 73, no. 12, pp. 19 140–19 155, 2024.

[20] C. Zhang, M. Cui, and G. Zhang, "Throughput optimization for IRS-assisted multi-user NOMA URLLC systems," *Wireless Networks*, vol. 29, no. 6, pp. 2505–2517, April 2023.

[21] G. Li, M. Zeng, D. Mishra, L. Hao, Z. Ma, and O. A. Dobre, "Energy-efficient design for IRS-empowered uplink MIMO-NOMA systems," *IEEE Transactions on Vehicular Technology*, vol. 71, no. 9, pp. 9490–9500, 2022.

[22] M. Zeng, E. Bedeer, O. A. Dobre, P. Fortier, Q.-V. Pham, and W. Hao, "Energy-efficient resource allocation for IRS-assisted multi-antenna uplink systems," *IEEE Wireless Communications Letters*, vol. 10, no. 6, pp. 1261–1265, 2021.

[23] X. Yu, G. Wang, X. Huang, K. Wang, W. Xu, and Y. Rui, "Energy efficient resource allocation for uplink RIS-aided millimeter-wave networks with NOMA," *IEEE Transactions on Mobile Computing*, vol. 23, no. 1, pp. 423–436, 2024.

[24] T. Qiao, Y. Cao, J. Tang, N. Deng, N. Zhao, and Y. Li, "Energy efficiency maximization for active IRS-assisted uplink NOMA systems," *IEEE Wireless Communications Letters*, vol. 13, no. 6, pp. 1561–1565, 2024.

[25] Z. Xu, J. Liu, J. Zou, and Z. Wen, "Energy-efficient design for IRS-assisted NOMA-based mobile edge computing," *IEEE Communications Letters*, vol. 26, no. 7, pp. 1618–1622, 2022.

[26] H. Wang, C. Liu, Z. Shi, Y. Fu, and R. Song, "Power minimization for uplink RIS-assisted CoMP-NOMA networks with GSIC," *IEEE Transactions on Communications*, vol. 70, no. 7, pp. 4559–4573, 2022.

[27] W. Dinkelbach, "On nonlinear fractional programming," *Management Science*, vol. 13, no. 7, pp. 492–498, 1967.

[28] Z. Yang, M. Chen, W. Saad, W. Xu, M. Shikh-Bahaei, H. V. Poor, and S. Cui, "Energy-efficient wireless communications with distributed reconfigurable intelligent surfaces," *IEEE Transactions on Wireless Communications*, vol. 21, no. 1, pp. 665–679, 2022.

[29] A. Hoorfar and M. Hassani, "Inequalities on the lambert function and hyperpower function," *JIPAM. Journal of Inequalities in Pure Applied Mathematics*, vol. 9, no. 2, pp. 5–9, 2008.

[30] E. U. T. R. Access, "Further advancements for E-UTRA physical layer aspects," *3GPP Technical Specification TR*, vol. 36, p. V2, 2010.

[31] B. Zheng and R. Zhang, "Intelligent reflecting surface-enhanced OFDM: Channel estimation and reflection optimization," *IEEE Wireless Communications Letters*, vol. 9, no. 4, pp. 518–522, 2020.

[32] C. You, B. Zheng, and R. Zhang, "Channel estimation and passive beamforming for intelligent reflecting surface: Discrete phase shift and progressive refinement," *IEEE Journal on Selected Areas in Communications*, vol. 38, no. 11, pp. 2604–2620, 2020.

[33] Z.-Q. He and X. Yuan, "Cascaded channel estimation for large intelligent metasurface assisted massive MIMO," *IEEE Wireless Communications Letters*, vol. 9, no. 2, pp. 210–214, 2020.

[34] M. Zeng, X. Li, G. Li, W. Hao, and O. A. Dobre, "Sum rate maximization for IRS-assisted uplink NOMA," *IEEE Communications Letters*, vol. 25, no. 1, pp. 234–238, 2021.

[35] Z. Wei, L. Yang, D. W. K. Ng, J. Yuan, and L. Hanzo, "On the performance gain of NOMA over OMA in uplink communication systems," *IEEE Transactions on Communications*, vol. 68, no. 1, pp. 536–568, 2020.

[36] M. Vaezi, R. Schober, Z. Ding, and H. V. Poor, "Non-orthogonal multiple access: Common myths and critical questions," *IEEE Wireless Communications*, vol. 26, no. 5, pp. 174–180, 2019.

[37] M. Naeem, K. Illanko, A. Karmokar, A. Anpalagan, and M. Jaseemuddin, "Optimal power allocation for green cognitive radio: fractional programming approach," *IET Communications*, vol. 7, no. 12, pp. 1279–1286, 2013.

[38] C. Isheden, Z. Chong, E. Jorswieck, and G. Fettweis, “Framework for link-level energy efficiency optimization with informed transmitter,” *IEEE Transactions on Wireless Communications*, vol. 11, no. 8, pp. 2946–2957, 2012.

[39] M. Di Renzo, A. Zappone, T. T. Lam, and M. Debbah, “System-level modeling and optimization of the energy efficiency in cellular networks—a stochastic geometry framework,” *IEEE Transactions on Wireless Communications*, vol. 17, no. 4, pp. 2539–2556, 2018.

[40] A. Zappone, M. Di Renzo, and R. K. Fotock, “Surface-based techniques for IoT networks: Opportunities and challenges,” *IEEE Internet of Things Magazine*, vol. 5, no. 4, pp. 72–77, 2022.

[41] E. Björnson and E. G. Larsson, “How energy-efficient can a wireless communication system become?” in *2018 52nd Asilomar Conference on Signals, Systems, and Computers*, October 2018, pp. 1252–1256.

BIOGRAPHIES OF AUTHORS

El-Hadi Meftah completed his M.Sc. in electronics and communication engineering at USTHB in Algiers, Algeria, in 2009. He later earned his Ph.D. in electronics engineering from the University Saad Dahleb of Blida, Algeria. From 2010 to 2013, he served as an instructor at Eloued University in Algeria, and from 2013 to 2022 at Chlef University, also in Algeria. Currently, he holds the position of lecturer in the Department of Electronics Engineering at USTHB university. His research focuses on various aspects of wireless communications, including topics such as NOMA, MIMO/RIS/LIS systems. He can be contacted at email: emeftah@usthb.dz.

Slimane Benmahmoud received the BS from M'sila university, the MS and the PhD from Djillali liabes university in Algeria. From 2010 to 2012, he was employed as an instructor at El-oued university in Algeria. He was a visiting research scholar to north carolina state universiy (NCSU) in the USA, from 2014 to 2016, where he conducted research on convex optimisation, and cooperative communications. He is currently a lecturer in the department of Electronics Engineering at M'sila university. His main research interests are in coded modulation, convex optimisation and cooperative communications. He can be contacted at email: slimane.benmahmoud@univ-msila.dz.